Classification Based on Texture Analysis for Synthetic Hazy Image from Mount Kelud Haze Image Density

Fresy Nugroho
Informatics Engineering, Faculty of Science and Technology
Universitas Islam Negeri Maulana Malik Ibrahim
Malang, Indonesia
fresy@ti.uin-malang.ac.id

Puspa Miladin Safitri A. Basid
Informatics Engineering, Faculty of Science and Technology
Universitas Islam Negeri Maulana Malik Ibrahim
Malang, Indonesia
puspa.miladin@uinmalang.ac.id

Yunifa Miftachul Arif
Informatics Engineering, Faculty of Science and Technology
Universitas Islam Negeri Maulana Malik Ibrahim
Malang, Indonesia
yunif4@ti.uin-malang.ac.id

Norizan Mat Diah
Universiti Teknologi MARA
Shah Alam, Malaysia
norizan289@uitm.edu.my

Firma Sahrul Bahtiar
Library and Information Science, Faculty of Science and Technology
Universitas Islam Negeri Maulana Malik Ibrahim
Malang, Indonesia
firma.sb@uin-malang.ac.id

Fardani Annisa Damastuti
Multimedia Creative Technology Departement
Politeknik Elektronika Negeri Surabaya
Surabaya, Indonesia
fardani@pens.ac.id

Fachrul Kurniawan
Informatics Engineering, Faculty of Science and Technology
Universitas Islam Negeri Maulana Malik Ibrahim
Malang, Indonesia
fachrulk@ti.uin-malang.ac.id

Nurizal Dwi Priandani
Informatics Engineering, Faculty of Science and Technology
Universitas Islam Negeri Maulana Malik Ibrahim
Malang, Indonesia
nd.priandani@uin-malang.ac.id

Dodik Arwin Dermawan
Manajemen Informatika Program Vokasi
Universitas Negeri Surabaya
Surabaya, Indonesia
dodikdermawan@unesa.ac.id

***Abstract*—This paper classifies the simulations of homogeneous synthetic images, heterogeneous synthetic hazy images, and original hazy images taken from CCTV (Close Circuit Television) of Mt. Kelud crater using the GLCM (Gray Level Co-Occurrence Matrix) method. The average feature values obtained using the GLCM (Gray Level Co-Occurrence Matrix) method are used to compare the similarity of gray feature values of the three and then classify thin, medium, and thick images. The results for classifying thin haze, medium haze, and thick haze on the homogeneous synthetic hazy image test data obtained an accuracy value of 50%, a precision value of 46%, and a sensitivity value of 65%. As for the classification of thin, medium, and thick fog on heterogeneous synthetic hazy images, test data obtained an accuracy value of 42%, a precision value of 32%, and a sensitivity value of 48%.**

Keywords—Operator, Tipografi, Profesi, Lorem, Ipsum

I. INTRODUCTION

Virtual environments [1]–[3] have been produced and used in several industries, including games[4], [5]. The computer-simulated environment aims to build a real world that matches human senses, including touch, hearing, sight, taste, and smell [6], [7]. Some of the natural phenomena that were successfully virtualized include rain[8], snow[9], water[10] and haze[11].

Some researchers assert that synthetic haze is needed to simulate the process of haze in the real world [12]. Sarker used artificial haze to validate haze removal techniques in an image [13]. The use of synthetic haze was also further investigated by Husain to determine the range of view after removing the haze in the image[14]. Wang's research proposed illumination settings by considering colour to remove synthetic haze and smoke in images with fire scenarios[15]. Meanwhile, Hassan's observation examines the effects of haze and haze removal on deep learning-based vision models[16].

However, the research on synthetic fog that several researchers have conducted still needs to involve classification. Classification is crucial, starting with Balaa's research, which proposed a classification of user interactions in virtual environments for mobile devices [17]. Another researcher, Albert, and Sung, proposed a user-centered classification[18]. Their research supports the findings of Minhas et al., where their research successfully performed weather classification by applying synthetic data [19]. Some haze classification work has been done by Zhao, whose research proposed haze removal based on haze degree classification [20]. Another researcher, Ngo et al., proposed a haze removal system based on haze condition calibration [21].

The use of classification using GLCM has been applied to various problems, for example, for road damage detection [22], building cracks caused by earthquakes [23], wayang images [24], the quality of guava leaf types for treatment [25], the quality of coffee beans [26], the utilization of tumor image features [27], and the signals generated by the brain through Magnetic Resonance Imaging [28].

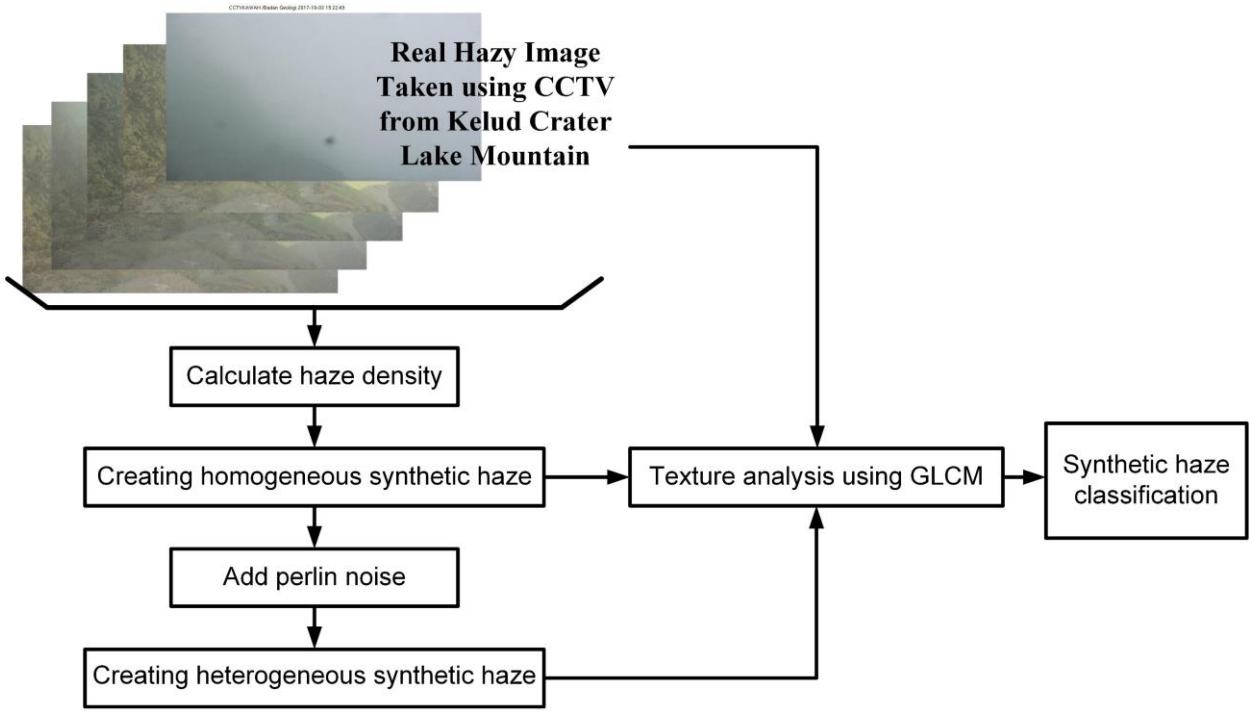

Fig 1. Block Diagram System for Synthetic Haze Classification.

A classification based on texture analysis utilizing GLCM at a hazy synthetic image is suggested in light of the research mentioned above gaps. Based on the haze level over the Kelud Mount crater lake, this study can categorize and identify synthetic haze. The experiment outcomes demonstrated that the synthetic haze's categorization performance has a significant impact. The GLCM successfully categorizes and identifies the many kinds of synthetic haze produced by our research. It can serve as a starting point for further investigating the hazy density distribution features.

II. Experimental Design

This research consists of several steps, starting with collecting hazy images of the crater lake of Mount Kelud, then calculating the haze density, followed by making a homogeneous synthetic haze. This homogeneous synthetic haze is added with Perlin noise to produce a heterogeneous synthetic haze. Three kinds of images, namely hazy images of the crater lake of Mount Kelud, homogeneous synthetic haze, and heterogeneous synthetic haze, are analyzed using a grey-level co-occurrence matrix to classify hazy images. System design using the GLCM method in this study, as shown in figure 1.

A. Collecting Hazy Images of The Crater Lake of Mount Kelud

The hazy image of the crater lake of Mount Kelud was obtained from CCTV permanently installed on Mount Kelud, with the camera's direction facing the crater lake, and the camera was activated continuously for 24 hours. However, in this study, only visible images were selected from 06.00 am to 05.00 pm. Image recording was done every 5 minutes. Thus, the image recording done in a day is 12 hours.

In taking image data from CCTV of Mount Kelud, 12 images were obtained every hour, so 144 images were obtained daily. Because the image recording was carried out for two days, 288 images of the hazy crater lake of Mount Kelud were obtained. Each recorded image was labeled to distinguish the recording. The label attached to each image contains the date of recording and the time of recording. This label has a white background. So for the haze density calculation process, this label needs to be removed first so as not to cause ambiguous haze density calculations as shown in figure 2. The image size used in this study is 800 x 400 pixels in JPG format, as shown in figure 3. The CCTV sensor belongs to the Center for Volcanology and Geological Hazard Mitigation (PVMBG) of Mount Kelud in the Kediri district, East Java, with the Axis Q1755-E model, which has a resolution of 1280 x 720 pixels.

Fig 2. Hazy Images of The Crater Lake of Mount Kelud without label

Fig 3. Hazy Images of The Crater Lake of Mount Kelud.

B. Calculating the Haze Density

FADE (Haze Aware Density Evaluator) is a patron designed to predict the appearance or clarity of images hidden by haze. It can perform forecasting by not referring to haze-free images, not relying on dominant entities in hazy images, not considering depth-based transmission maps, and not requiring human evaluation(Choi et al. 2015). FADE takes advantage of the deviation from statistical harmony observed in hazy and haze-free images. FADE predicts the perceptual thinness of the haze phenomenon for the image as a whole. The thin thickness predicted using FADE is closely related to the human evaluation of haze density.

The observed haze characteristics based on the NSS (Natural Scane Statistic) patron are a light color, contrast, and light shift. The NSS patron considers computation, and contrast is normalized by MSCN (Mean Subtracted Contrast Normalized). The statistical characteristics of the hazy image used consist of 12 types. These features include the variety of MSCN coeval, a variety of the sheer amount of MSCN coefficient consisting of 2 features (positive, negative mode), sharpening, a coeval of variety of sharpening, contradiction energy consisting of 3 features (greyscale, yellow-blue, and red-green), image entropy, dark channel prior, color saturation, colorfulness.

Haze density calculation was performed by applying the fog aware density evaluator to hazy images of the crater lake of Mount Kelud. The images obtained from Mount Kelud were recorded every 5 minutes, from 6:00 am to 5:00 pm, for two days. Then the hourly average was calculated. The results of the average haze density calculation are shown in Table 1. Based on the calculation of the average haze density, it is known that the low value of haze density is at 08.00 am, with a haze density value of 2,410, while the highest haze density value occurs at 03.00 pm, which is worth 8,181. The average value of haze density in a day is 3,970. Based on Table 1, it can also be seen that the haze in Mount Kelud's crater always changes its density value.

TABLE I. HAZE DENSITY OF KELUD MOUNTAIN CRATER LAKE.

Time	*Density*
06.00 AM	3.554
07.00 AM	3.373
08.00 AM	**2.410**
09.00 AM	3.424
10.00 AM	4.108
11.00 AM	3.257
12.00 PM	2.761
01.00 PM	4.208
02.00 PM	3.092
03.00 PM	**8.181**
04.00 PM	5.123
05.00 PM	4.154
Average	3.970

C. Homogeneous Synthetic Haze

The haze phenomenon has the following mathematical model:

$$I(x) = J(x)t(x) + \big(1 - t(x)\big)\mathrm{A} \qquad (1)$$

Where $J(x)$ is the scene radiance or image without fog for each pixel x, $t(x) \in [0,1]$ is the transmission map of the reflected light in the atmosphere, and A is the skylight representing the light in the atmosphere. $J(x)t(x)$ shows how the medium attenuates the scene radiance. While $\big(1 - t(x)\big)\mathrm{A}$ is the airlight.

Furthermore, the transmission map is defined as the inverse of the depth map. Transmission occurs due to the scattering process that passes through fog particles with various β conditions, then reaches the observer point formulated as follows:

$$t(x) = exp\left(-\int_0^{d(x)} \beta(z)dz\right) \qquad (2)$$

Where β is the light scattering coefficient, d is the depth map, and $t(x)$ is the transmission map that describes a portion of the scattered light that passes through particles in the air. Alternatively, it can be written in the form of the following equation:

$$t(x) = e^{-\beta d(x)} \qquad (3)$$

Based on the fog density value obtained, a two-dimensional homogeneous synthetic fog is created by adjusting the coefficient β by applying the density parameter λ in equation (3) so that equation (4) is obtained as follows:

$$t(x)^{\lambda} = (e^{-\beta d(x)})^{\lambda} = e^{-(\lambda\beta)d(x)} \qquad (4)$$

By applying equation (4) to equation (1), the mathematical model of homogeneous synthetic haze is obtained:

$$J_{homogeneous}(x) = J(x)t(x)^{\lambda} + \big(1 - t(x)^{\lambda}\big)\mathrm{A} \qquad (5)$$

D. Heterogeneous Synthetic Haze

However, the haze phenomenon in the real world is only sometimes perfectly homogeneous. Therefore, this research applies Perlin noise to produce a more natural heterogeneous synthetic fog. This process can be written in a mathematical formula:

$$R(x) = J_{homogeneous}(x) + k * n(x) \qquad (6)$$

The value of $R(x)$ is the heterogeneous synthetic haze, while $J_{homogeneous}(x)$ is the homogeneous synthetic haze in equation (5). In equation (6), the value of $R(x)$ is the result achieved from applying equation (4) to equation (7), thus equation (8) is obtained:

$$J_{homogeneous}(x) = \frac{I(x) - A}{\max\,(t(x),\ t_0)} \qquad (7)$$

$$J_{homogeneous}(x) = \frac{I(x) - A}{\max\,(t(x)^{\lambda},\ t_0)} \qquad (8)$$

So equation (6) can be rewritten as :

$$R(x) = \frac{I(x) - A}{\max\,(t(x)^{\lambda},\ t_0)} + k * n(x) \qquad (9)$$

E. *Classify Hazy Images*

The GLCM features used for classification in this study are :

Energy:

$$energy = \sum_{i1} \sum_{12} p^2 (i_1, i_2) \quad (10)$$

Correlation:

$$correlation = \sum_{i1} \sum_{i2} \frac{(i_1 - \mu_1)(i_2 - \mu_2)}{\sigma_{i1}\sigma_{i2}} \quad (11)$$

Contrast:

$$contrast = \sum_{i1} \sum_{i2} (i_1 - i_2)^2 p(i_1, i_2) \quad (12)$$

Homogenity:

$$homogenity = \sum_{i1} \sum_{i2} \frac{p(i_1, i_2)}{1 + |i_1 - i_2|} \quad (13)$$

In the above four equations, the notation p represents the probability of an element in the co-occurrence matrix. Whereas i_1 and i_2 represent adjacent intensity pairs, the co-occurrence matrix is the row and column numbers, respectively.

III. RESULT

This section describes the implementation of GLCM measurement of the homogeneous synthetic foggy image, the heterogeneous foggy image implementation, and the fog-free image. Then the clacification results are based on GLCM features and the confusion matrix results.

A. *Homogeneous Synthetic Haze*

Figure 4 below is a simulation based on the transmission map according to equation (5) and the density value generated and shown in Table 1. The homogeneous synthetic hazy image simulation produces 12 images by considering the average hourly haze density data.

Fig 4. Homogeneous Synthetic Haze Images.

B. *Heterogeneous Synthetic Haze*

Figure 5 below is a simulation by applying Perlin noise according to equation (9) with density values following Table 1. The simulation of the heterogeneous synthetic hazy image produced 12 images by considering the average hourly haze density data.

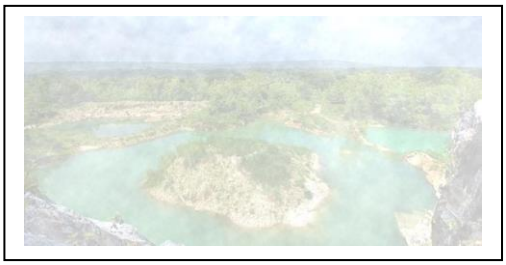

Fig 5. Heterogeneous Synthetic Haze Images.

A. *Coordinate Pair Test Location.*

The experiment was conducted by analyzing the texture value using the GLCM method (based on the average result of the combination of four statistical features at degrees 0, 45, 90, and 135 by taking into account the pixel distance of d = 2. In each foggy image, an image of 100x100 pixels was selected. Each piece of image is located at five different coordinate pairs. Then the results obtained are averaged so that the value of the texture feature can be identified. The five points include: (1) Coordinate (100,100), (2) Coordinate (250,60), (3) Coordinate (5,220), (4) Coordinate (315,200), and (5) Coordinate (500,60). The five coordinates are shown in the figure 6 below.

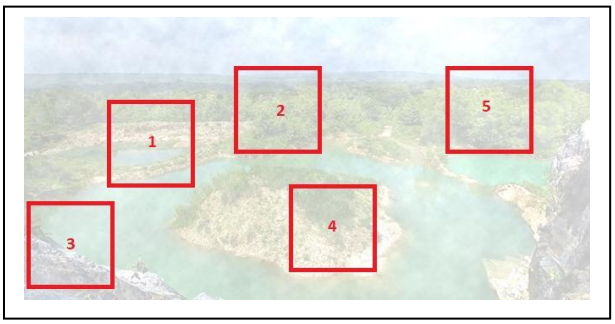

Fig 6. Coordinate pair test location of an image.

B. *Value of GLCM Features*

The values of the average GLCM calculation result of the hazy image in Mount Kelud's crater lake are shown in Table 2, the homogeneous synthetic hazy image is shown in Table 3, and the calculation result of the heterogeneous hazy image is shown in Table 4 respectively.

TABLE II. THE AVERAGE GLCM VALUES OF FIVE TIME TEST EXPERIMENTS ON THE HAZY IMAGE IN MOUNT KELUD'S CRATER LAKE.

Time	*CON*	*CORR*	*EN*	*HOM*
06.00 AM	0,133	0,765	0,765	0,430
07.00 AM	0,115	0,772	0,772	0,474
08.00 AM	0,356	0,551	0,351	0,365
09.00 AM	0,169	0,644	0,644	0,520
10.00 AM	0,177	0,596	0,596	0,476
11.00 AM	0,204	0,635	0,635	0,395
12.00 PM	0,175	0,727	0,727	0,401
01.00 PM	0,148	0,622	0,622	0,494
02.00 PM	0,135	0,653	0,653	0,511
03.00 PM	0,017	0,928	0,928	0,991
04.00 PM	0,126	0,702	0,702	0,511
05.00 PM	0,122	0,716	0,716	0,539

TABLE III. THE AVERAGE GLCM VALUES OF FIVE TIME TEST EXPERIMENTS ON THE HOMOGENEOUS HAZY IMAGE

Time	*CON*	*CORR*	*EN*	*HOM*
06.00 AM	0,106	0,521	0,664	0,947
07.00 AM	0,094	0,445	0,715	0,952
08.00 AM	0,215	0,458	0,471	0,893
09.00 AM	0,098	0,454	0,702	0,950
10.00 AM	0,154	0,538	0,517	0,923
11.00 AM	0,087	0,372	0,395	0,956
12.00 PM	0,126	0,359	0,675	0,937
01.00 PM	0,167	0,529	0,490	0,930
02.00 PM	0,086	0,3291	0,751	0,956
03.00 PM	0,001	-0,004	0,999	0,999
04.00 PM	0,204	0,536	0,398	0,897
05.00 PM	0,158	0,533	0,506	0,920

TABLE IV. THE AVERAGE GLCM VALUES OF FIVE TIME TEST EXPERIMENTS ON THE HETEROGENEOUS HAZY IMAGE

Time	*CON*	*CORR*	*EN*	*HOM*
06.00 AM	0,126	0,425	0,644	0,936
07.00 AM	0,084	0,521	0,732	0,957
08.00 AM	0,168	0,534	0,483	0,915
09.00 AM	0,111	0,452	0,656	0,944
10.00 AM	0,024	0,233	0,940	0,987
11.00 AM	0,137	0,465	0,588	0,931
12.00 PM	0,195	0,546	0,419	0,902
01.00 PM	0,008	0,135	0,978	0,99
02.00 PM	0,172	0,547	0,466	0,913
03.00 PM	0,001	-0,002	0,998	0,999
04.00 PM	0,007	0,077	0,998	0,999
05.00 PM	0,066	0,233	0,821	0,967

After conducting experiments for the hazy image in mount Kelud's crater lake, the homogeneous hazy synthetic images, and the heterogeneous hazy synthetic images are classified into three groups based on their GLCM feature values. The three groups are thin, medium, and thick haze. The example of the haze image classification shown in Table 5.

TABLE V. THE CLASSIFICATION OF THE HAZY IMAGE IN MOUNT KELUD'S CRATER LAKE BASED ON GLCM

CON	*CORR*	*EN*	*HOM*	*Classification*
0,133	0,765	0,765	0,430	medium
0,115	0,772	0,772	0,474	medium
0,356	0,551	0,351	0,365	thin
0,169	0,644	0,644	0,520	medium
0,177	0,596	0,596	0,476	thin
0,204	0,635	0,635	0,395	medium
0,175	0,727	0,727	0,401	medium
0,148	0,622	0,622	0,494	medium
0,135	0,653	0,653	0,511	medium
0,017	0,928	0,928	0,991	thick
0,126	0,702	0,702	0,511	medium
0,122	0,716	0,716	0,539	medium

The classification of the hazy image in Mount Kelud'scrater Lake results determines the reference value of each feature of the four features produced in the original foggy image shown in Table 6.

TABLE VI. THE REFERENCE FEATURES VALUES FOR CLASSIFICATION OF THIN, MEDIUM, AND THICK HAZY IMAGE IN MOUNT KELUD'S CRATER LAKE BASED ON GLCM

	GLCM Features	**Haze Classification**		
		Thin	*Medium*	*Thick*
Value	*CON*	>=0,2	0,1-0,19	<0,1
	CORR	<0,6	0,6-0,7	>=0,8
	EN	<0,4	0,4-0,5	>=0,6
	HOM	<0,85	0,86-0,95	>=0,96

The classification of thin, medium, and thick haze on homogeneous and heterogeneous hazy images at each hour from 06.00 am to 05.00 pm is shown in Tables 7 and 8, respectively.

TABLE VII. THE CLASSIFICATION OF THIN, MEDIUM AND THICK IN HOMOGENEOUS SYNTHETIC HAZY IMAGE BASED ON GLCM

Time	**Image Number**	**Original Data Classification**	**Manual Data Classification**
06.00 AM	1	medium	medium
07.00 AM	2	medium	thick
08.00 AM	3	thin	thin
09.00 AM	4	medium	thick
10.00 AM	5	thin	medium
11.00 AM	6	medium	thin
12.00 PM	7	medium	medium
01.00 PM	8	medium	medium
02.00 PM	9	medium	thick
03.00 PM	10	thick	thick
04.00 PM	11	medium	thin
05.00 PM	12	medium	medium

TABLE VIII. THE CLASSIFICATION OF THIN, MEDIUM AND THICK IN HETEROGENEOUS SYNTHETIC HAZY IMAGE BASED ON GLCM

Time	**Image Number**	**Original Data Classification**	**Manual Data Classification**
06.00 AM	1	medium	medium
07.00 AM	2	medium	thick
08.00 AM	3	thin	medium
09.00 AM	4	medium	medium
10.00 AM	5	thin	thick
11.00 AM	6	medium	thin
12.00 PM	7	medium	medium
01.00 PM	8	medium	thick
02.00 PM	9	medium	medium
03.00 PM	10	thick	thick
04.00 PM	11	medium	thick
05.00 PM	12	medium	thick

Furthermore, a confusion matrix calculation is performed to find the value of accuracy, precision, and sensitivity of the homogeneous synthetic hazy image. The confusion matrix of homogeneous synthetic hazy images was collected in Table 9. After calculating the confusion matrix in the homogeneous synthetic hazy images data, it can be seen that the accuracy of the test data has an accuracy value of 50%, a precision value of 46%, and a sensitivity value of 65%.

The confusion matrix calculation to find the value of accuracy, precision, and sensitivity of the heterogeneous synthetic hazy image is shown in Table 10. From the confusion matrix in the heterogeneous synthetic hazy images data, it can be seen that the accuracy of the test data has an accuracy value of 42%, a precision value of 32%, and a sensitivity value of 48%.

TABLE IX. CONCLUSION MATRIX CALCULATION OF THE HOMOGENEOUS SYNTHETIC HAZY IMAGE BASED ON GLCM COMPARE TO HAZY IMAGE IN MOUNT KELUD'S CRATER LAKE

		Actual		
		Thin	**Medium**	**Thick**
Prediction	**Thin**	1	2	0
	Medium	1	4	0
	Thick	0	3	1

TABLE X. CONCLUSION MATRIX CALCULATION OF THE HETEROGENEOUS SYNTHETIC HAZY IMAGE BASED ON GLCM COMPARE TO HAZY IMAGE IN MOUNT KELUD'S CRATER LAKE

	Actual			
Prediction		**Thin**	**Medium**	**Thick**

	Thin	0	1	0
	Medium	1	4	0
	Thick	1	4	1

V. CONCLUSION

In this study, the three have similar feature values to homogeneity features between the hazy image, the homogeneous synthetic hazy image, and the heterogeneous synthetic hazy image. In the energy feature, the hazy image is similar to the feature's value with a homogeneous synthetic hazy image. Whereas, for contrast and correlation features, the homogeneous synthetic hazy image has similar feature values to the heterogeneous synthetic hazy image. In the results of the haze classification using the GLCM features values, the accuracy value resulting from the classification of the homogeneous synthetic hazy image is higher than that of the heterogeneous synthetic hazy image.

ACKNOWLEDGEMENT

This research is financially supported by the State Higher Education Operational Assistance Financing Program (BOPTN) Decree of the Rector of UIN Maulana Malik Ibrahim Malang, Number 674 of 2023. We express our deepest gratitude to all leaders and laboratory assistants in the Faculty of Science and Technology, UIN Maulana Malik Ibrahim, Malang.

REFERENCES

[1] C. Juliantino, M. P. Nathania, R. Hendarti, H. Darmadi, and B. A. Suryawinata, "The development of virtual healing environment in VR platform," *Procedia Comput Sci*, vol. 216, pp. 310–318, 2023, doi: 10.1016/j.procs.2022.12.141.

[2] M. Newman, B. Gatersleben, K. J. Wyles, and E. Ratcliffe, "The use of virtual reality in environment experiences and the importance of realism," *J Environ Psychol*, vol. 79, p. 101733, 2022, doi: https://doi.org/10.1016/j.jenvp.2021.101733.

[3] J. Huang and S. Li, "Research on the Application of Digital VR Technology in Snow and Ice Landscape Teaching," *J Phys Conf Ser*, vol. 1992, no. 2, p. 22122, Aug. 2021, doi: 10.1088/1742-6596/1992/2/022122.

[4] F. Nugroho, E. M. Yuniarno, and M. Hariadi, "An Environmental Domain Awareness for Serious-Game Using Perlin Noise Base Heterogeneous Haze Visualization," *International Journal of Intelligent Engineering and Systems*, vol. 15, no. 2, 2022, doi: 10.22266/ijies2022.0430.25.

[5] Y. M. Arif, S. Harini, S. M. S. Nugroho, and M. Hariadi, "An Automatic Scenario Control in Serious Game to Visualize Tourism Destinations Recommendation," *IEEE Access*, vol. 9, pp. 89941–89957, 2021, doi: 10.1109/ACCESS.2021.3091425.

[6] T. Jantakoon, P. Wannapiroon, and P. Nilsook, "Virtual Immersive Learning Environments (VILEs) Based on Digital Storytelling to Enhance Deeper Learning for Undergraduate Students," *Higher Education Studies*, vol. 9, May 2019, doi: 10.5539/hes.v9n1p144.

[7] C. Chunpungsuk, P. Chatwattana, and P. Piriyasurawong, "Effect of Backward Design With Virtual Learning Ecosystem to Enhance Design Thinking and Innovation Skills," *Research in World Economy*, vol. 12, no. 4, p. 70, Sep. 2021, doi: 10.5430/rwe.v12n4p70.

[8] S. Hasirlioglu and A. Riener, "A General Approach for Simulating Rain Effects on Sensor Data in Real and Virtual Environments," *IEEE Transactions on Intelligent Vehicles*, vol. 5, no. 3, pp. 426–438, 2020, doi: 10.1109/TIV.2019.2960944.

[9] J. Huang and X. Zhou, "Interactive application of VR technology in ice and snow landscape design," *J Phys Conf Ser*, vol. 1744, no. 3, p. 32100, Feb. 2021, doi: 10.1088/1742-6596/1744/3/032100.

[10] S. Lu, C. Fang, and X. Xiao, "Virtual Scene Construction of Wetlands: A Case Study of Poyang Lake, China," *ISPRS Int J Geoinf*, vol. 12, no. 2, 2023, doi: 10.3390/ijgi12020049.

[11] X. Jin, R. Tang, L. Liu, and J. Wu, "Vehicle license plate recognition for fog-haze environments," *IET Image Process*, vol. 15, May 2021, doi: 10.1049/ipr2.12103.

[12] R. Sheikh, A. Sarker, and M. S. Uddin, "Simulation of Haze on Real World Images with Generative Adversarial Network Trend Forecasting of Dhaka Stock Exchange Using Machine Learning Techniques View project A Skin Disease Detection System View project," 2019, doi: 10.13140/RG.2.2.27677.74727.

[13] A. Sarker, M. Akter, and M. S. Uddin, "Simulation of Hazy Image and Validation of Haze Removal Technique," *Journal of Computer and Communications*, vol. 07, no. 02, pp. 62–72, 2019, doi: 10.4236/jcc.2019.72005.

[14] N. A. Husain, M. S. M. Rahim, S. Kari, and H. Chaudhry, "VRHAZE: The Simulation of Synthetic Haze Based on Visibility Range for Dehazing Method in Single Image," in *2020 6th International Conference on Interactive Digital Media (ICIDM)*, 2020, pp. 1–7. doi: 10.1109/ICIDM51048.2020.9339638.

[15] C. Wang, J. Hu, X. Luo, M. P. Kwan, W. Chen, and H. Wang, "Color-Dense Illumination Adjustment Network for Removing Haze and Smoke from Fire Scenario Images," *Sensors*, vol. 22, no. 3, Feb. 2022, doi: 10.3390/s22030911.

[16] H. Hassan, P. Mishra, M. Ahmad, A. K. Bashir, B. Huang, and B. Luo, "Effects of haze and dehazing on deep learning-based vision models," *Applied Intelligence*, 2022, doi: 10.1007/s10489-022-03245-5.

[17] E. Balaa, M. Raynal, Y. Bou Issa, and E. Dubois, "LNCS 8525 - Classification of Interaction Techniques in the 3D Virtual Environment on Mobile Devices," 2014.

[18] J. Albert and K. Sung, "User-Centric Classification of Virtual Reality Locomotion," 2018, doi: 10.1145/3281505.

[19] S. Minhas, Z. Khanam, S. Ehsan, K. McDonald-Maier, and A. Hernández-Sabaté, "Weather Classification by Utilizing Synthetic Data," *Sensors*, vol. 22, no. 9, May 2022, doi: 10.3390/s22093193.

[20] X. Zhao, T. Zhang, W. Chen, and W. Wu, "Image Dehazing Based on Haze Degree Classification," in *Proceedings - 2020 Chinese Automation Congress, CAC 2020*, Institute of Electrical and Electronics Engineers Inc., Nov. 2020, pp. 4186–4191. doi: 10.1109/CAC51589.2020.9327091.

[21] D. Ngo, S. Lee, G. D. Lee, and B. Kang, "Automating a dehazing system by self-calibrating on haze conditions," *Sensors*, vol. 21, no. 19, Oct. 2021, doi: 10.3390/s21196373.

[22] R. H. Pramestya, D. R. Sulistyaningrum, B. Setiyono, I. Mukhlash, and Z. Firdaus, "Road defect classification using Gray Level Co-Occurrence Matrix (GLCM) and Radial Basis Function (RBF)," in *Proceedings of 2018 10th International Conference on Information Technology and Electrical Engineering: Smart Technology for Better Society, ICITEE 2018*, Institute of Electrical and Electronics Engineers Inc., Nov. 2018, pp. 285–289. doi: 10.1109/ICITEED.2018.8534769.

[23] I. G. Pasek Suta Wijaya, C. Sulton, I. B. Ketut Widiartha, and N. Nyoman Kencanawati, "Building Crack Due To Lombok Earthquake Classification Based on GLCM Features and SVM Classifier," in *2019 International Conference on Advanced Mechatronics, Intelligent Manufacture and Industrial Automation (ICAMIMIA)*, 2019, pp. 91–96. doi: 10.1109/ICAMIMIA47173.2019.9223403.

[24] M. Muhathir, M. H. Santoso, and D. A. Larasati, "Wayang Image Classification Using SVM Method and GLCM Feature Extraction," *JOURNAL OF INFORMATICS AND TELECOMMUNICATION ENGINEERING*, vol. 4, no. 2, pp. 373–382, Jan. 2021, doi: 10.31289/jite.v4i2.4524.

[25] S. Ibad, W. H. Suristiyanti, M. N. A. Farah, N. Rijati, and C. Supriyanto, "Application of Grayscale Co-occurrence Matrix (GLCM) Method for Classification of Quality Type of Guava Leaves as Traditional Medicine Using Neural Network Algorithm," in *2022 International Seminar on Application for Technology of Information and Communication (iSemantic)*, 2022, pp. 310–313. doi: 10.1109/iSemantic55962.2022.9920397.

[26] M. Jumarlis, ; Mirfan, ; Abdul, and R. Manga, "Classification of coffee bean defects using gray-level co-occurrence matrix and k-nearest neighbor," *ILKOM Jurnal Ilmiah*, vol. 14, no. 1, pp. 1–9, 2022, doi: 10.33096/ilkom.v14i1.910.1-9.

[27] J. Alyami *et al.*, "Cloud Computing-Based Framework for Breast Tumor Image Classification Using Fusion of AlexNet and GLCM Texture Features with Ensemble Multi-Kernel Support Vector Machine (MK-SVM)," *Comput Intell Neurosci*, vol. 2022, pp. 1–9, Aug. 2022, doi: 10.1155/2022/7403302.

[28] C. T. Selvi, R. S. Sankarasubramanian, and S. Karthikeyani, "Multikernel Support Vector Machine with GLCM For Truthful Brain Signal Classification of Magnetic Resonance Imaging," in *2022 8th International Conference on Advanced Computing and Communication Systems (ICACCS)*, 2022, pp. 246–251. doi: 10.1109/ICACCS54159.2022.9785363.